ACCSCIENCE PUBLISHING

Eurasian Journal of Medicine and Oncology

ORIGINAL RESEARCH ARTICLE

Bioinformatic identification of a fatty acid metabolism-related gene signature for prognosis prediction and drug sensitivity assessment in osteosarcoma

Hao Gu[1†], Changsheng Zhang[1†], Yu Li[1], Chuanzhi Zhang[2], Xiao Shi[1*], and Xinxin Si[1*]

[1]Jiangsu Key Laboratory of Marine Pharmaceutical Compound Screening, Jiangsu Key Laboratory of Marine Biotechnology, Co-Innovation Center of Jiangsu Marine Bio-industry Technology, School of Pharmacy, Jiangsu Ocean University, Lianyungang, Jiangsu, China

[2]Bio-Pharmaceutical Research Institute, Lian Yun Gang Chia Tai Tianqing Pharmaceutical Group Co., Ltd, Lianyungang, Jiangsu, China

Abstract

Introduction: Osteosarcoma is an aggressive malignancy with high metastatic potential, leading to poor prognosis in recurrent and metastatic cases.

Objectives: This study aimed to identify prognostic fatty acid metabolism-related genes (FAMRGs) in osteosarcoma and characterize the clinical and biological features of *ACSF2*.

Methods: Transcriptomic and clinical data from Therapeutically Applicable Research to Generate Effective Treatments–Osteosarcoma, Genotype-Tissue Expression, and GSE16088 were analyzed. Consistently differentially expressed FAMRGs were screened via dual-cohort validation. Least absolute shrinkage and selection operator and Cox regression analyses were used to select prognostic genes, with overall survival (OS) as the primary endpoint and event-free survival (EFS) as the secondary endpoint. An ACSF2-based prognostic model combined with metastatic status was internally validated by bootstrap resampling. Gene Set Enrichment Analysis, OncoPredict, ESTIMATE, and CIBERSORT analyses were performed to explore *ACSF2*-associated pathways, drug sensitivity, and immune infiltration. *In vitro* functional assays were conducted to verify the biological function of acyl-CoA synthetase family member 2 (ACSF2).

Results: Four prognostic FAMRGs were screened from 15 consistently dysregulated genes. Low *ACSF2* expression independently predicted inferior OS and EFS, without significant correlation with diagnostic metastasis. The optimized model yielded a corrected C-index of 0.729 and a calibration slope of 0.943. ACSF2 was closely associated with fatty acid and mitochondrial metabolism. The *ACSF2*-high subgroup showed higher predicted sensitivity to Uprosertib and MN-64 and exhibited distinct immune infiltration patterns. Functional experiments confirmed that elevated *ACSF2* expression suppresses the migration and invasion of human osteosarcoma cells.

Conclusion: *ACSF2* is a promising candidate prognostic biomarker for osteosarcoma. Its metabolic, pharmacological, and immune correlations are exploratory and require further experimental validation.

Keywords: *ACSF2*; Fatty acid metabolism; Prognostic biomarker; Osteosarcoma

[†]*These authors contributed equally to this work.*

***Corresponding authors:**
Xiao Shi
(xiaoshi@jou.edu.cn);
Xinxin Si
(sixx@jou.edu.cn)

Citation: Gu H, Zhang C, Li Y, Zhang C, Shi X, Si X. Bioinformatic identification of a fatty acid metabolism-related gene signature for prognosis prediction and drug sensitivity assessment in osteosarcoma. *Eurasian J Med Oncol*.
doi: 10.36922/EJMO026310397

Received: July 29, 2026

Revised: September 21, 2026

Accepted: October 27, 2026

Published online: November 17, 2026

Copyright: © 2026 Author(s). This is an Open-Access article distributed under the terms of the Creative Commons Attribution License, permitting distribution, and reproduction in any medium, provided the original work is properly cited.

Publisher's Note: AccScience Publishing remains neutral with regard to jurisdictional claims in published maps and institutional affiliations.

1. Introduction

Osteosarcoma arises from transformed mesenchymal cells that produce aberrant osteoid and immature bone matrix.[1] Current standard therapy consists of radical surgical resection combined with multi-agent perioperative chemotherapy, which substantially improves outcomes for patients with localized disease.[2] Nevertheless, osteosarcoma is characterized by aggressive local invasion and a striking predilection for early hematogenous dissemination, predominantly pulmonary metastasis.[3] Approximately 30%–50% of patients experience tumor recurrence, and 20%–30% present with detectable metastatic lesions at initial diagnosis.[4] Clinically, patients with localized osteosarcoma achieve a five-year survival rate of approximately 60%–70%, whereas the prognosis deteriorates drastically to below 25% for individuals with metastatic or recurrent disease.[5] Notably, therapeutic breakthroughs over the past several decades have failed to significantly improve the survival of advanced osteosarcoma patients.[6] The lack of reliable prognostic biomarkers and effective targeted therapeutics highlights an urgent clinical need to identify novel molecular signatures to refine risk stratification and optimize treatment strategies.

Metabolic reprogramming is a core hallmark of malignant tumors and supports persistent tumor growth, invasive progression, and therapeutic resistance.[7] Lipid metabolic remodeling, in particular, enables cancer cells to adapt to stressful microenvironmental conditions and actively modulates tumor immune landscapes by regulating the proliferation, infiltration, and functional polarization of immune cells.[8] Multiple lipid metabolic enzymes and transporters have been validated as actionable oncogenic drivers and therapeutic targets across various malignancies. For example, pharmacological inhibition of 3-hydroxy-3-methylglutaryl-CoA reductase by statins disrupts de novo cholesterol synthesis, deprives tumor cells of essential metabolic substrates, and suppresses malignant progression.[9] Targeting lipid metabolism has therefore emerged as a promising strategy for tumor intervention.

Fatty acid metabolism constitutes a core subprogram of lipid metabolic reprogramming, supporting sustained tumor proliferation, invasive growth, redox homeostasis, and immune microenvironment remodeling across multiple malignancies.[10] In osteosarcoma, dysregulated fatty acid metabolism has been increasingly recognized as a critical driver of malignant progression, enabling tumor cells to adapt to metabolic stress, promote distant metastasis, and shape an immunosuppressive tumor microenvironment.[11,12] Emerging evidence indicates that altered fatty acid metabolic signatures are closely correlated with clinical prognosis and immune infiltration in osteosarcoma.[13] However, most current studies focus on overall lipid metabolism rather than systematic profiling of fatty acid metabolism-related genes (FAMRGs). In particular, acyl-CoA synthetase family member 2 (ACSF2), a key enzyme responsible for fatty acid activation and acyl-CoA metabolic regulation, occupies an upstream and essential position in fatty acid metabolism. Nevertheless, the prognostic value, immune regulatory roles, and biological functions of ACSF2 in osteosarcoma remain largely uncharacterized. Against this background, the present study systematically screened dysregulated FAMRGs in multi-cohort osteosarcoma datasets, constructed a FAMRG-based prognostic signature, and further focused on ACSF2 to explore its clinical implications and tumor-modulating function via bioinformatic validation and in vitro functional experiments. This work aims to provide novel metabolic biomarkers and potential therapeutic clues for osteosarcoma.

2. Materials and methods

2.1. Data collection

Log_2-transformed transcripts per million expression matrices of Therapeutically Applicable Research to Generate Effective Treatments–Osteosarcoma (TARGET-OS) and Genotype-Tissue Expression (GTEx) skeletal muscle tissues were downloaded from the University of California, Santa Cruz (UCSC) Xena database. Among 88 TARGET-OS samples with available transcriptomic profiles, 84 samples with complete clinical information (Table S1) were included for subsequent analyses. Consistent with previous osteosarcoma transcriptomic studies,[14-17] GTEx skeletal muscle samples were utilized as non-tumor control tissues. The normalized series matrix of GSE16088 was retrieved from the Gene Expression Omnibus database.

Differential expression analysis was independently performed in the TARGET-OS/GTEx cohort and the GSE16088 cohort using the R package *limma* (version 3.60.6). Given that expression matrices from different datasets were analyzed separately without integration, cross-platform batch correction was not performed. Genes with a nominal $p < 0.05$ and $|\log_2 FC| \geq 1$ were identified in each cohort. Only FAMRGs with consistent differential expression patterns across the two cohorts were retained for further analysis. Multiple testing correction was not applied at this exploratory screening stage.

A total of 176 unique FAMRGs were derived from the REACTOME_FATTY_ACID_METABOLISM gene set in the Molecular Signatures Database (MSigDB, version 7.5.1, Broad Institute of MIT and Harvard, USA), as listed in Table S2. This manually curated gene set covers core genes involved in multiple biological processes of fatty

acid metabolism, including fatty acid activation, synthesis, elongation, degradation, and β-oxidation.

2.2. Protein–protein interaction networks analysis

We extracted protein–protein interaction information for those dysregulated FAMRGs using the Search Tool for the Retrieval of Interacting Genes/Proteins database (version 12.0), and the constructed interaction networks were further visualized via Cytoscape (version 3.10.2, Cytoscape Consortium, USA). The MCODE plugin (version 2.0.3) was applied to identify core hub modules, and hub genes within key modules were selected for subsequent analyses.

2.3. Functional enrichment analysis

We implemented Gene Ontology (GO) and Kyoto Encyclopedia of Genes and Genomes (KEGG) enrichment analyses utilizing *clusterProfiler* (v4.12.6) in R. GO enrichment results covered three categories: biological process, cellular component, and molecular function. Enriched terms with a nominal $p < 0.05$ were visualized via circular and bubble plots. No multiple-testing correction was performed at this step; therefore, all enrichment results were interpreted as preliminary and exploratory.

2.4. Screening of prognostic fatty acid metabolism-related genes

We performed least absolute shrinkage and selection operator (LASSO) Cox regression analysis targeting the 15 differentially expressed FAMRGs using the R package *glmnet* (v4.1–8) to identify candidate genes with prognostic value. The stability of gene selection was assessed by 500 bootstrap resamplings with five-fold cross-validation implemented in each resample. Survival analyses used the *survival* (v3.8–3) and *survminer* (v0.5.0) packages in R. The primary endpoint was overall survival (OS), evaluated using the survival times and vital status recorded in TARGET-OS. The secondary endpoint, event-free survival (EFS), was evaluated using the recorded EFS times and first-event information. For EFS analysis, tumor relapse, patient death, or the occurrence of a second malignant neoplasm was regarded as a clinical event, whereas patients without events were censored. We constructed Kaplan-Meier survival curves for prognostic comparison among subgroups stratified by gene expression levels. For each gene, the expression cut-off was selected with *maxstat* (version 0.7–25) using maximally selected rank statistics. Because the cut-offs were selected and evaluated in the same TARGET-OS cohort, the survival comparisons require cautious interpretation, and the cut-offs should not be treated as independently validated clinical thresholds.

2.5. Cox regression and prognostic model construction

Associations of gene-expression groups and clinical covariates with OS were examined using univariable and multivariable Cox proportional hazards models. Metastatic status was defined as the presence of metastasis at diagnosis rather than subsequent metastatic progression or relapse. The multivariable models included sex, age, metastatic status, definitive surgery, and gene-expression group as covariates. For prognostic model construction, *ACSF2* expression was entered as a continuous variable and combined with metastatic status at diagnosis. Using the *rms* package (v7.0-0), we developed a nomogram to estimate OS probabilities at 1, 3, and 5 years and generated calibration curves to compare the predictions with observed outcomes. Time-dependent ROC analyses were implemented via *timeROC* (v0.4). We conducted internal validation for this two-variable fixed model with 1,000 bootstrap resampling replicates. Coefficients were refitted in every bootstrap sample. We calculated optimism-corrected estimates of Harrell's C-index, the calibration slope, and time-dependent area under the curves for years 1, 3, and 5.

2.6. Gene set enrichment analysis

For pathway analysis, the median *ACSF2* expression in TARGET-OS was used to define the *ACSF2*-high and *ACSF2*-low groups. Genes were ranked by the $\log_2$ fold change between the two expression groups, and Gene Set Enrichment Analysis (GSEA) was run in clusterProfiler using GO and KEGG gene sets from MSigDB. *p*-values were adjusted for multiple testing using the Benjamini–Hochberg procedure. Gene sets satisfying false discovery rate-adjusted $p < 0.05$ were displayed as clustered networks using the *enrichplot* R package (v1.24.4). These analyses identify pathways associated with *ACSF2* expression but do not establish that *ACSF2* directly regulates them.

2.7. Predicted drug-response analysis

We used the *oncoPredict* R package (version 1.2) to estimate transcriptome-based drug-response scores using Genomics of Drug Sensitivity in Cancer 2 pharmacogenomic training data. The predicted scores were transformed as $\log_2(x+1)$, with lower values indicating greater predicted sensitivity. Scores were compared between groups defined by the median *ACSF2* expression level using the Wilcoxon rank-sum test. Compounds showing between-group differences at nominal $p < 0.05$ were selected for exploratory follow-up. Spearman correlations were then calculated between *ACSF2* expression and their predicted response scores.

2.8. Tumor microenvironment and immune cell composition analysis

Stromal, immune, and ESTIMATE scores were computed based on TARGET-OS transcriptomic datasets with the R package *estimate* (v1.0.13). The relative proportions of 22 immune-cell populations were inferred from bulk RNA-seq data by applying the CIBERSORT R script (v1.03). We used Wilcoxon rank-sum tests to compare estimated scores and immune-cell fractions between ACSF2 groups defined by median expression. We calculated Pearson correlations of *ACSF2* expression with the estimated immune-cell fractions and the expression of immune-related genes. These findings were interpreted as computational estimates rather than direct measurements of immune-cell infiltration.

2.9. Cell culture and transfection

The culture medium for human osteosarcoma (HOS) cells was Dulbecco's Modified Eagle Medium supplemented with 10% fetal bovine serum (FBS; Gibco, USA) and 1% penicillin–streptomycin. Cultures were kept at 37 °C under humidified conditions with 5% CO_2. Transfection was performed when the plated HOS cells reached 70% confluence. HOS cells were transiently transfected with either a plasmid encoding full-length human ACSF2 or the empty vector using Lipofectamine (Invitrogen, USA), following the supplier's protocol. In short, plasmids and transfection reagent were separately diluted in serum-free medium, incubated at ambient temperature to generate transfection complexes, and carefully dispensed into cell culture medium. Cells were collected for functional assays 48–72 h after transfection.

2.10. Colony formation assay

For colony formation, transfected cells were seeded at low density in six-well plates and cultured for 7–10 days. Visible colonies were fixed with 4% paraformaldehyde and then stained with crystal violet. Colony counts were quantified to assess the proliferative potential of cells.

2.11. Transwell invasion assay

Matrigel-coated Transwell inserts were used for the invasion assay. We added the cell suspension to the upper chamber and medium containing 10% FBS to the lower chamber, where FBS served as the chemoattractant. After 36 h of incubation, cells that had invaded through the membrane were fixed and stained. Invasion was assessed by counting the cells that had crossed the membrane.

2.12. Wound healing

When cells attained full monolayer confluence, we generated a uniform linear wound. Phosphate-buffered saline washing was performed to discard detached floating cells, followed by medium replacement with serum-free culture medium. Imaging was performed at 0 h and 16 h. The scratch closure area was quantified to assess the migratory potential of cells.

2.13. Western blot

For protein extraction, transfected HOS cells were lysed in ice-cold radioimmunoprecipitation assay buffer containing a protease inhibitor cocktail. Protein concentrations in the lysates were measured with a bicinchoninic acid assay kit (BL521A, Biosharp, China) following the supplier's protocol. Sodium dodecyl sulfate–polyacrylamide gel electrophoresis was used to resolve samples containing equal amounts of protein, followed by electrophoretic transfer to polyvinylidene fluoride membranes. After blocking, the membranes were exposed to an anti-ACSF2 primary antibody (1:500; 16140-1-AP, Proteintech, USA) at 4 °C overnight. The membranes were then washed with Tris-buffered saline with Tween 20 and incubated for 1 h with horseradish peroxidase-conjugated secondary antibodies. Following another round of Tris-buffered saline with Tween 20 washes, the bands were detected by enhanced chemiluminescence. Protein signals were normalized to glyceraldehyde-3-phosphate dehydrogenase, which served as the loading control.

2.14. Statistical analysis

All statistical computations were carried out in R software (version 4.4.1, R Foundation for Statistical Computing, Austria). Two-sided statistical tests were adopted for all analyses unless otherwise specified, and a threshold of $p < 0.05$ was defined as the cut-off for statistical significance. Differential expression screening, GO and KEGG enrichment, computational drug response prediction, immune cell abundance comparisons, and immune-associated correlation analyses relied on unadjusted nominal *p*-values without correction for multiple testing; these results were interpreted as exploratory. Corrections for maximally selected rank statistics were computed and presented independently.

3. Results

3.1. Identification of differentially expressed fatty acid metabolism-related genes

Differential expression analyses were independently conducted in the GSE16088 and TARGET-OS/GTEx datasets. Heatmaps displaying the top 50 differentially expressed genes ranked by nominal *p*-values from each cohort are presented in Figure 1A and 1B. By intersecting these differentially expressed genes with the 176 FAMRGs

(Table S2), we identified 15 FAMRGs with consistent expression alterations across the two datasets, including seven concordantly upregulated and eight concordantly downregulated genes (Figure 1C and 1D). Paired volcano plots further validated the consistent differential expression patterns of these candidate FAMRGs in the two independent cohorts (Figure 1E). The seven upregulated FAMRGs included *ACSL3*, *PTGES3*, *PPT1*, *PLA2G4A*, *HSD17B12*, *PON2*, and *ACLY*, while the eight downregulated FAMRGs were *ACSF2*, *DECR2*, *ACADS*, *ACAA1*, *AKR1C3*, *CYP2J2*, *EPHX2*, and *ACOX2*.

3.2. Functional analysis of differentially expressed fatty acid metabolism-related genes

An expanded protein interaction network was generated in the Search Tool for the Retrieval of Interacting Genes/Proteins using the 15 differentially expressed FAMRGs as seeds (Figure 2A). We ranked the proteins by interaction score and visualized the 50 highest-scoring proteins in Cytoscape (Figure 2B). Downstream GO and KEGG enrichment showed predominant enrichment of these genes within fatty-acid degradation, fatty acid metabolism,

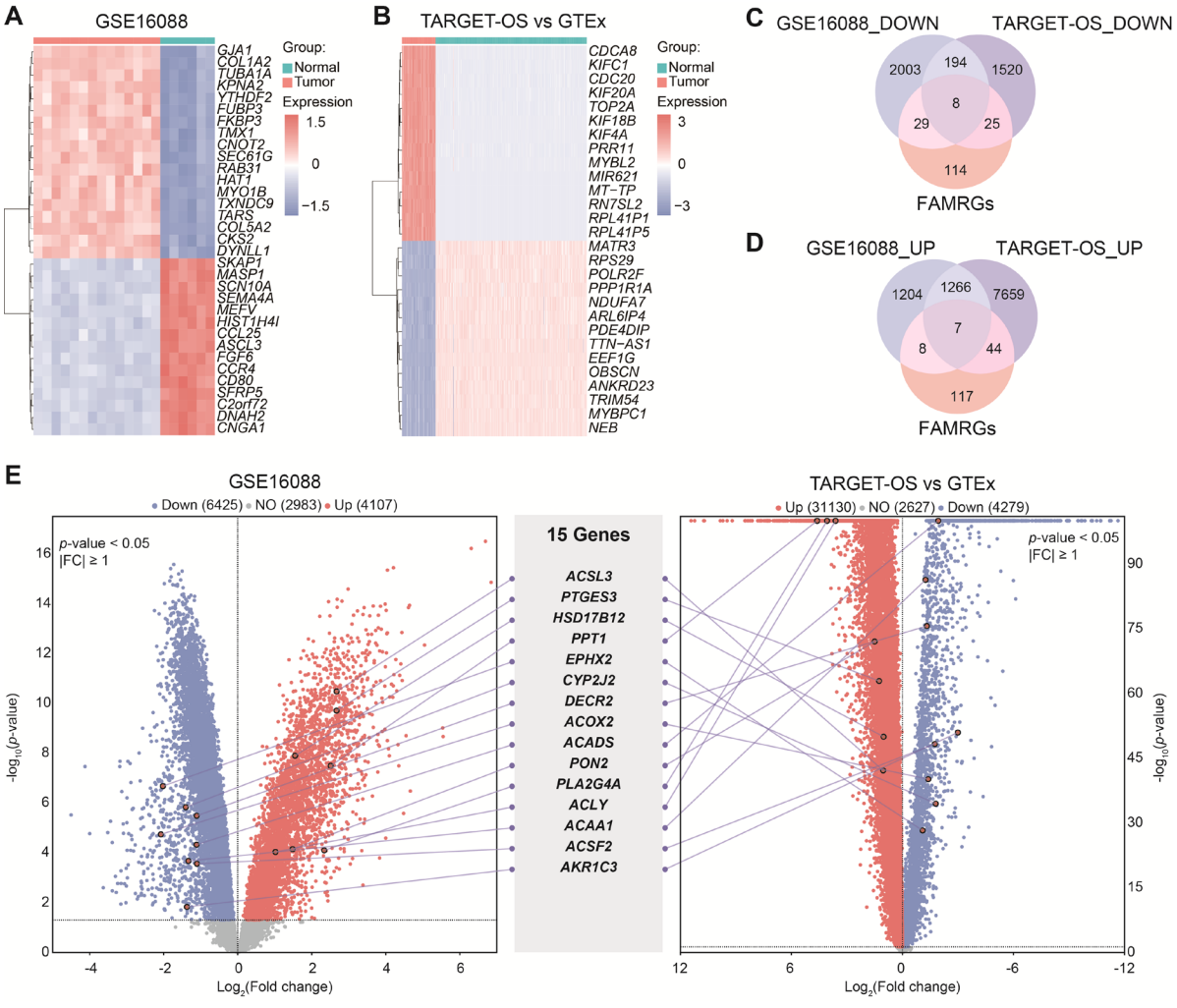


Figure 1. Screening of differentially expressed fatty acid metabolism-related genes (FAMRGs). Heatmaps show the top 50 differentially expressed genes ranked by nominal *p*-value in (A) GSE16088 and (B) the Generate Effective Treatments–Osteosarcoma (TARGET-OS)/Genotype-Tissue Expression (GTEx) comparison. Venn diagrams identify FAMRGs showing concordant (C) downregulation and (D) upregulation in both datasets. (E) Volcano plots show the differentially expressed FAMRGs in GSE16088 and the TARGET-OS/GTEx comparison.
Note: Differential gene expression was defined by thresholds: nominal $^*p < 0.05$ and $|\log_2 FC| \geq 1$.

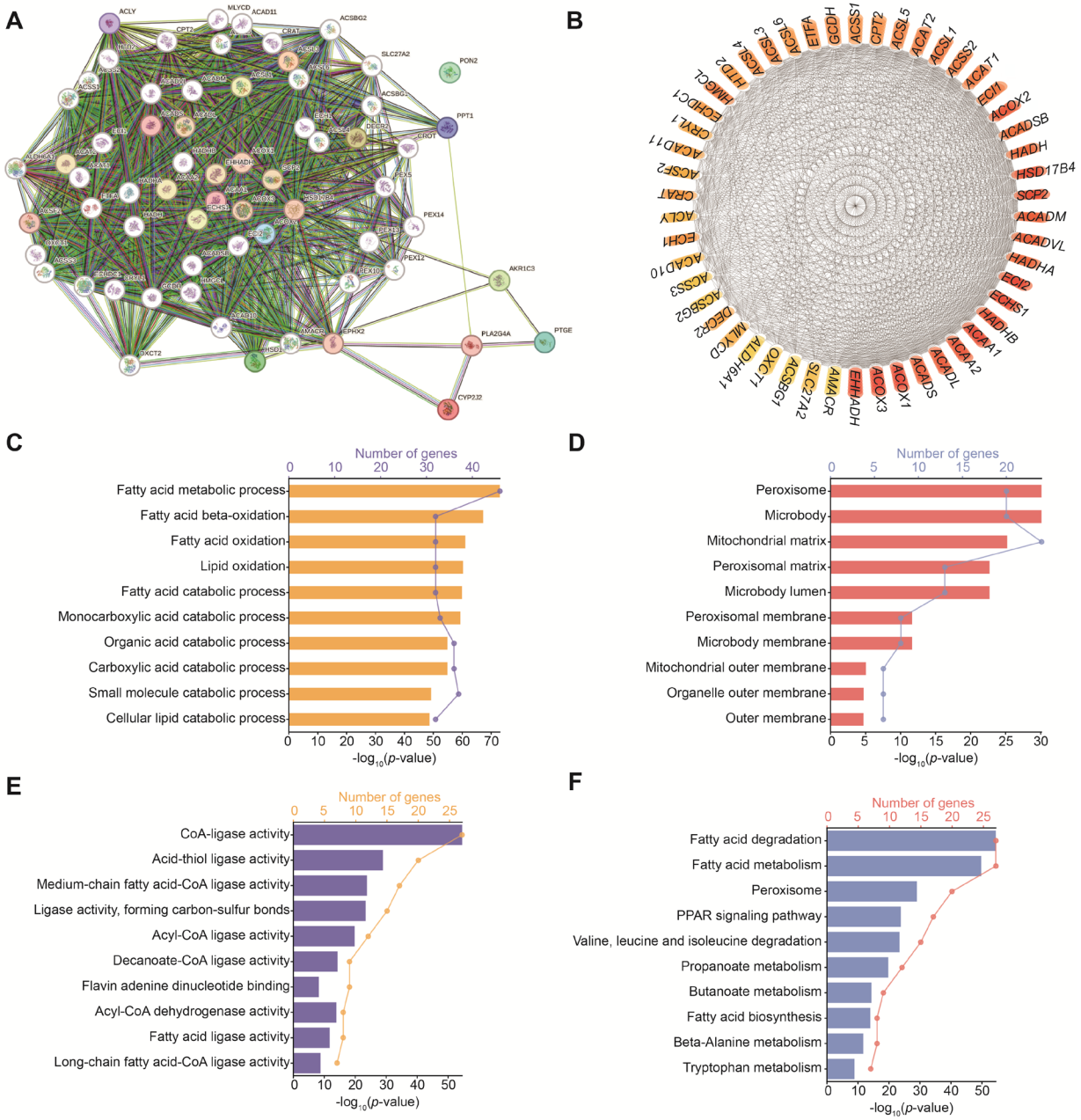


Figure 2. Biological characterization of altered-expression fatty acid metabolism-related genes (FAMRGs). (A) Expanded Search Tool for the Retrieval of Interacting Genes/Proteins protein–protein interaction network constructed using the 15 differentially expressed FAMRGs as seed proteins. (B) Network of the 50 proteins with the highest interaction scores, visualized using Cytoscape. Enrichment results for the selected proteins are presented by Gene Ontology (GO) category—biological process (C), cellular component (D), and molecular function (E)—and by Kyoto Encyclopedia of Genes and Genomes (KEGG) pathway (F). Bars represent –log10(*p*-value), and points represent the number of associated genes. No multiple-testing adjustment was applied to the GO/KEGG *p*-values; these enrichment findings are exploratory.

peroxisome function, the peroxisome proliferator-activated receptor signaling pathway, and valine, leucine, and isoleucine degradation (Figure 2C–F; nominal $p < 0.05$). Notably, we did not apply multiple-testing correction to any enrichment analyses at this step; therefore, these functional enrichment results are exploratory associations rather than definitive biological conclusions.

3.3. Screening of fatty acid metabolism-related genes with prognostic significance

The LASSO Cox regression was applied to the 15 differentially expressed FAMRGs for prognostic biomarker screening, from which four candidate genes were finally selected: *PPT1*, *ACSF2*, *EPHX2*, and *DECR2* (Figure 3A). Bootstrap stability testing with 500 resampling cycles showed *ACSF2* was preserved in 79.8% of regression models, reflecting robust selection stability in the TARGET-OS cohort. Expression profiling showed *PPT1* exhibited marked upregulation in osteosarcoma specimens, while *ACSF2*, *EPHX2*, and *DECR2* displayed persistent downregulation (Figure 3B). Kaplan–Meier survival curves revealed that patients belonging to the *ACSF2*-low subgroup had substantially poorer OS and EFS relative to individuals with high *ACSF2* expression (Figure 3C and 3D). Univariate Cox regression further verified that reduced *ACSF2* expression served as an unfavorable prognostic marker, associated with elevated mortality risk (hazard ratio [HR] = 2.78, 95% confidence interval [CI]: 1.29–5.97; $p = 0.009$) and higher EFS event risk (HR = 2.30, 95% CI: 1.17–4.54; $p = 0.016$). Since the optimal expression cut-off value was identified and validated solely within the TARGET-OS cohort, we interpreted these survival stratification findings cautiously.

3.4. Prognostic evaluation and model construction for *ACSF2*

The distributions of available clinical features across *ACSF2* and *PPT1* expression subgroups are presented in Figures

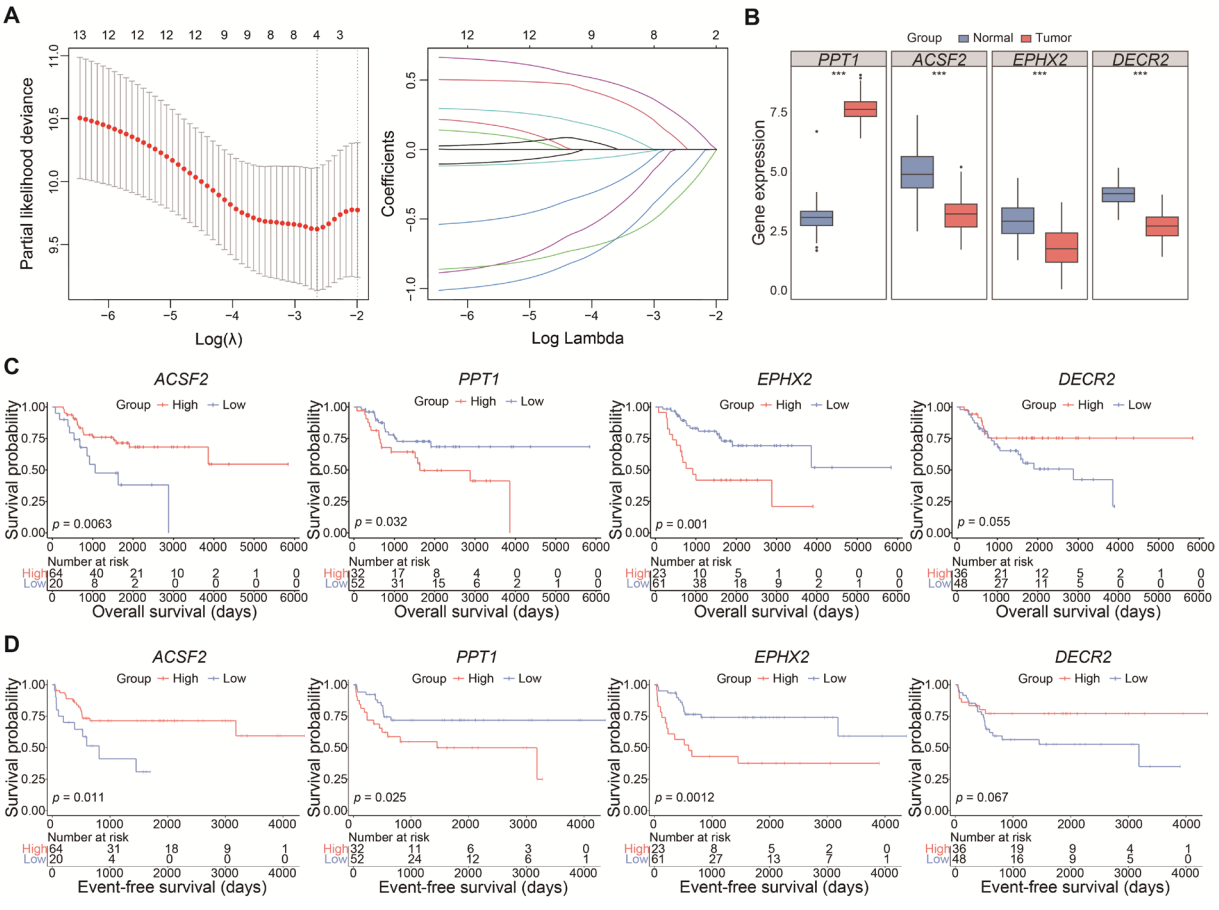


Figure 3. Screening of prognostic fatty acid metabolism-related genes (FAMRGs). (A) Cross-validation curve and coefficient profiles from least absolute shrinkage and selection operator Cox regression of the 15 differentially expressed FAMRGs. (B) Expression levels of *PPT1*, *ACSF2*, *EPHX2*, and *DECR2* in Generate Effective Treatments–Osteosarcoma (TARGET-OS) tumors and the Genotype-Tissue Expression non-tumor reference samples. (C) Overall survival and (D) event-free survival according to the expression groups of the four candidate genes in the 84-patient TARGET-OS cohort. Gene-expression subgroups were determined by maximally selected rank statistics; log-rank tests assessed survival disparities. Numbers at risk are shown below each Kaplan–Meier curve. The cut-offs were derived and evaluated in the same cohort and were not considered independently validated clinical thresholds.
Note: ***$p < 0.001$.

4A and S1A, respectively. Metastatic status here specifically denotes metastasis detected at the initial diagnosis. Among the total 84 enrolled patients, 22 exhibited metastatic lesions upon diagnosis. The metastatic rate tended to be greater among patients with low *ACSF2* expression relative to those with high *ACSF2* levels (8/20, 40.0% versus 14/64, 21.9%); nevertheless, this relationship lacked statistical significance (odds ratio = 2.35, 95% CI: 0.69–7.82; p = 0.145). Individual-level clinical and survival data for these 84 subjects are listed in Table S1, and Table 1 summarizes baseline clinical features stratified by vital status and *ACSF2*/*PPT1* expression subgroups.

Univariate Cox regression showed that metastasis at diagnosis correlated with increased mortality risk (HR = 3.96, 95% CI: 1.90–8.26; $p < 0.001$), whereas reduced *ACSF2* expression predicted worse OS (HR = 2.78, 95% CI: 1.29–5.97; p = 0.009) (Figure 4B). The multivariate model incorporated sex, age, metastatic status at diagnosis, definitive surgery, and *ACSF2* expression grouping. Within this adjusted model, metastasis at diagnosis (HR = 4.53, 95% CI: 2.04–10.06; $p < 0.001$) and low *ACSF2* abundance (HR = 2.38, 95% CI: 1.08–5.22; p = 0.031) remained independent predictors of increased death risk (Figure 4C). Univariate analysis also revealed that elevated *PPT1* expression was linked to higher mortality risk (HR = 2.19, 95% CI: 1.05–4.57; p = 0.037) (Figure S1B). However, this correlation lost statistical significance after multivariate adjustment (HR = 2.15, 95% CI: 0.99–4.65; p = 0.053) (Figure S1C). Accordingly, *PPT1* was excluded from the prognostic model and subsequent experimental validation, and all downstream analyses centered on *ACSF2*.

A prognostic model integrating continuous *ACSF2* expression levels and metastatic status at initial diagnosis was built to predict 1-, 3-, and 5-year OS (Figure 4D). Calibration curves were applied to contrast predicted versus observed OS probabilities (Figure 4E). The apparent time-dependent area under the curve values for all three time points were above 0.70 (Figure 4F). Internal validation based on 1,000 bootstrap resampling iterations generated an optimismadjusted Harrell's C-index of 0.729 alongside a calibration slope of 0.943, indicating a degree of internal stability within the TARGET-OS cohort.

Table 1. Clinical characteristics and gene-expression groups according to vital status in the Therapeutically Applicable Research to Generate Effective Treatments–Osteosarcoma cohort

Characteristics	Total, *n* (%)	Alive, *n* (%)	Dead, *n* (%)	*p*-value
Gender				0.571
Female	37 (44.05)	23 (41.82)	14 (48.28)	
Male	47 (55.95)	32 (58.18)	15 (51.72)	
Age				0.497
<18 years	66 (78.57)	42 (76.36)	24 (82.76)	
≥18 years	18 (21.43)	13 (23.64)	5 (17.24)	
Metastasis				<0.001
No	62 (73.81)	47 (85.45)	15 (51.72)	
Yes	22 (26.19)	8 (14.55)	14 (48.28)	
Definitive surgery				0.805
No	39 (46.43)	25 (45.45)	14 (48.28)	
Yes	45 (53.57)	30 (54.55)	15 (51.72)	
PPT1				0.019
High	32 (38.10)	16 (29.09)	16 (55.17)	
Low	52 (61.90)	39 (70.91)	13 (44.83)	
ACSF2				0.027
High	64 (76.19)	46 (83.64)	18 (62.07)	
Low	20 (23.81)	9 (16.36)	11 (37.93)	

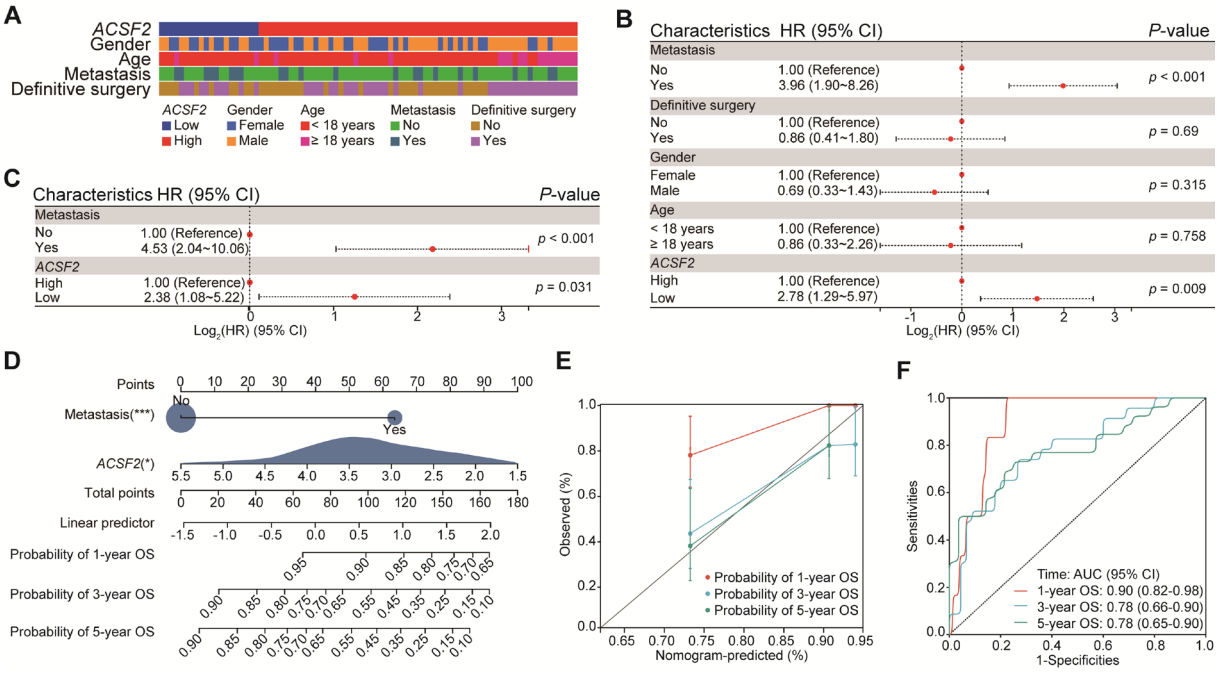


Figure 4. Prognostic evaluation and model construction for *ACSF2* in the Therapeutically Applicable Research to Generate Effective Treatments–Osteosarcoma cohort. (A) Distribution of *ACSF2* expression group, sex, age, metastasis at diagnosis, and definitive surgery among the 84 patients. The *ACSF2*-low and *ACSF2*-high groups included 20 and 64 patients, respectively. (B) Univariable Cox regression analysis of *ACSF2* expression group and the available clinical variables. (C) Multivariable Cox regression analysis of *ACSF2* expression group and metastatic status at diagnosis. Cox regression estimates are reported as hazard ratios (HR) with their 95% confidence intervals (CI). (D) Nomogram for estimating overall survival (OS) at 1, 3, and 5 years from continuous *ACSF2* expression and metastatic status at diagnosis. (E) Agreement between OS probabilities estimated by the nomogram and those observed in the cohort, assessed with calibration curves. (F) Receiver operating characteristic curves showing the model's time-dependent discrimination at 1, 3, and 5 years.
Notes: Metastasis refers to metastasis present at diagnosis. $^{*}p < 0.05$; $^{***}p < 0.001$.

3.5. Gene set enrichment analysis of *ACSF2*-associated pathways in osteosarcoma

The GSEA was conducted against GO entries (Figure 5A–C) and KEGG gene sets (Figure 5D) to uncover biological pathways correlated with ACSF2 expression. Following Benjamini–Hochberg multiple testing correction, gene sets with false discovery rate-adjusted $p < 0.05$ were kept and visualized via clustering network diagrams. The enriched signatures contained vascular endothelial growth factor and gonadotropin-releasing hormone signaling cascades, allograft rejection, fatty acid metabolic events, as well as mitochondrial energy-related processes. These findings reveal pathway-level correlations with *ACSF2* expression, though they cannot confirm direct regulatory effects exerted by *ACSF2*.

3.6. Predicted drug-response analysis associated with *ACSF2*

Exploratory transcriptome-based drug-response analysis identified nominal differences between the *ACSF2* expression groups for four compounds (Figure 6A). Predicted response scores for Acetalax (nominal $p = 0.030$), Uprosertib (nominal $p = 0.040$), and MN-64 (nominal $p = 0.027$) were lower in the *ACSF2*-high group than in the *ACSF2*-low group, suggesting greater predicted sensitivity. Entinostat showed the opposite pattern, with a higher predicted score in the *ACSF2*-high group (nominal $p = 0.042$), suggesting lower predicted sensitivity. *ACSF2* expression was negatively correlated with the predicted scores for Uprosertib (Spearman's $\rho = -0.23$, nominal $p = 0.039$) and MN-64 (Spearman's $\rho = -0.23$, nominal $p = 0.038$), whereas its correlations with Acetalax ($\rho = -0.11$, nominal $p = 0.320$) and Entinostat ($\rho = 0.14$, nominal $p = 0.190$) were not statistically significant (Figure 6B). Because multiple-testing correction was not applied, these findings were considered exploratory.

3.7. Associations between *ACSF2* expression and immune-related features

The *ACSF2*-high group had higher stromal and ESTIMATE

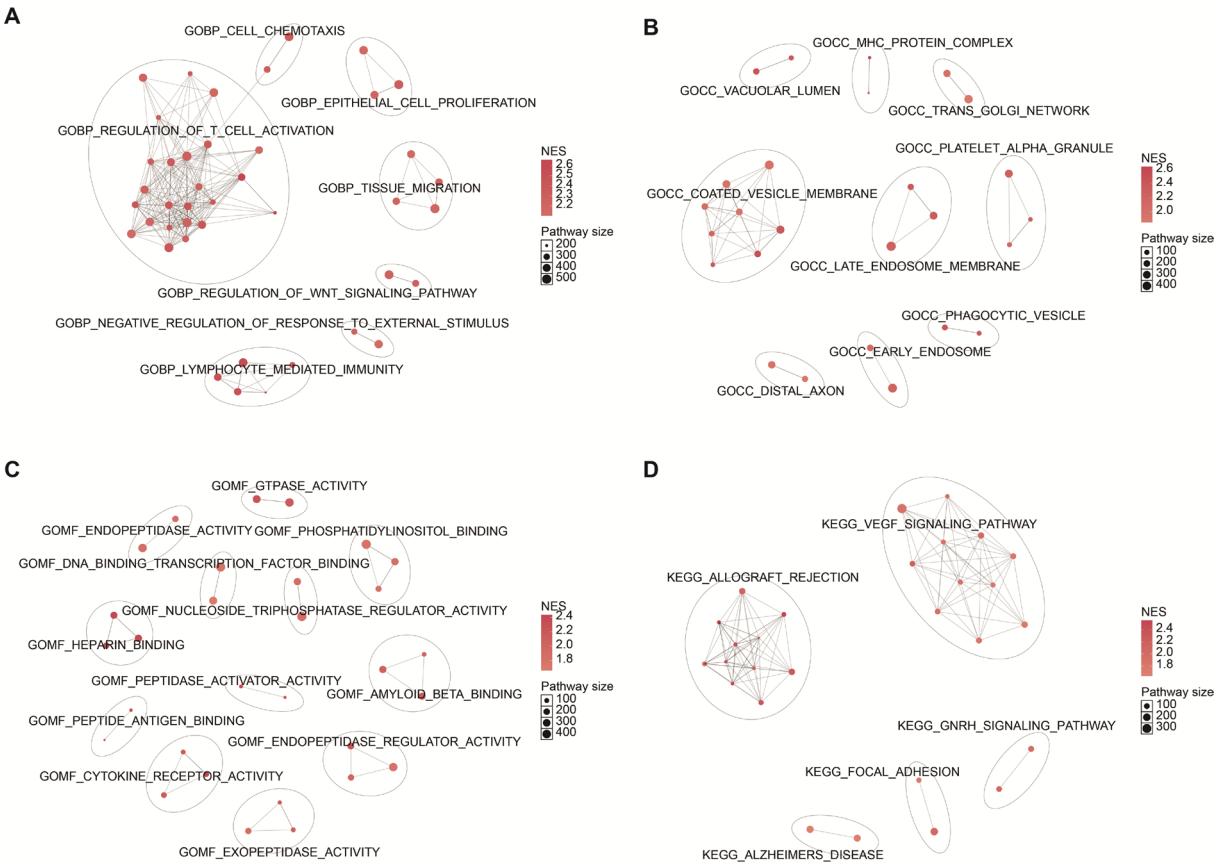


Figure 5. Gene set enrichment analysis of pathways associated with *ACSF2* expression. Enrichment networks are shown separately for the three Gene Ontology categories—biological process (A), cellular component (B), and molecular function (C)—and for Kyoto Encyclopedia of Genes and Genomes pathways (D). Nodes correspond to enriched gene sets, with links connecting sets that share genes. Node size indicates the total gene count of a set, while color indicates its normalized enrichment score (NES).

Notes: All displayed gene sets had a Benjamini–Hochberg false discovery rate-adjusted $p < 0.05$; these results indicate pathway-level associations and do not establish direct regulation by *ACSF2*.

scores than the *ACSF2*-low group, while the difference in immune scores was not statistically significant (Figure 7A). Relative fractions of 22 unique immune-cell subsets were computationally inferred from bulk RNA-seq data (Figure S2A). Comparisons of the estimated immune-cell proportions between the *ACSF2* expression groups are shown (Figure 7B). Pearson correlation coefficients describing the relationship between *ACSF2* abundance and predicted immune cell fractions are summarized in Figure 7C. *ACSF2* abundance exhibited an inverse correlation with the calculated proportion of regulatory T cells ($r = -0.23$, nominal $p = 0.042$) (Figure 7D). *ACSF2* expression was also negatively associated with *CCL21* and *TNFSF4* expression and positively associated with *ENTPD1* and *CCR10* expression (Figure S2B–F). These associations are exploratory because the *p*-values were not adjusted for multiple testing. The immune-cell fractions were inferred computationally and were not measured directly.

3.8. Acyl-CoA synthetase family member 2 inhibits the malignant phenotype of osteosarcoma cells

To characterize the tumor-suppressive bioactivity of ACSF2 in osteosarcoma, a panel of *in vitro* functional assays was performed. HOS cells were transfected with ACSF2 overexpression constructs or empty vector controls. Western blot was used to validate elevated ACSF2 protein abundance after transfection (Figure 8A). We then adopted wound-healing, Transwell invasion, and colony formation assays to assess oncogenic phenotypes of osteosarcoma cells. Our functional tests demonstrated that ectopic ACSF2 expression markedly impaired the migratory, invasive, and colony-forming capacity of HOS cells relative to vector-transfected control cells (Figure 8B–D).

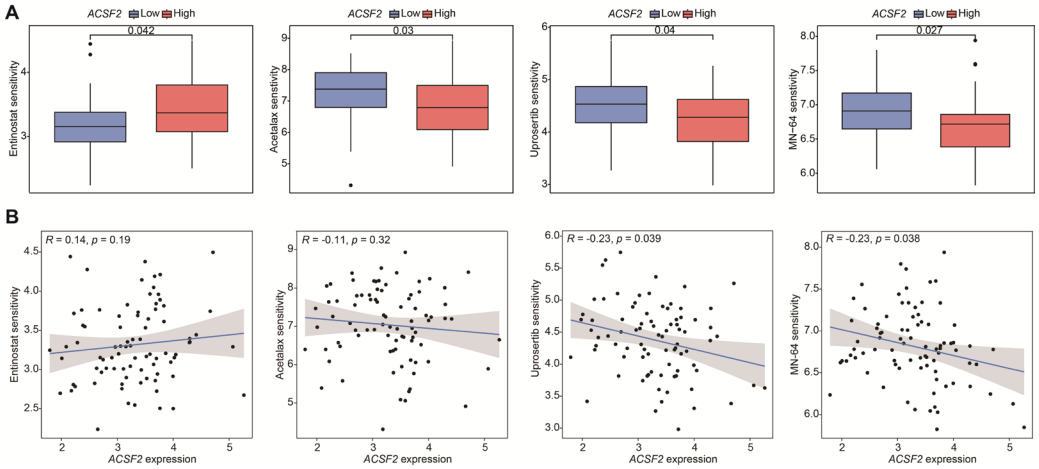


Figure 6. Exploratory analysis of predicted drug response in relation to *ACSF2* expression. (A) Comparison of predicted response scores for Entinostat, Acetalax, Uprosertib, and MN-64 between the median-defined *ACSF2*-low and *ACSF2*-high groups in the 84-patient Therapeutically Applicable Research to Generate Effective Treatments–Osteosarcoma cohort. The Wilcoxon rank-sum test was used for between-group comparisons. Lower response scores indicate greater predicted drug sensitivity. (B) Spearman-based correlation analysis of *ACSF2* expression against predicted response scores for the four tested agents. The shaded areas represent 95% confidence intervals.
Notes: *p*-values are nominal and were not adjusted for multiple comparisons; these transcriptome-based estimates do not represent observed drug responses in patients.

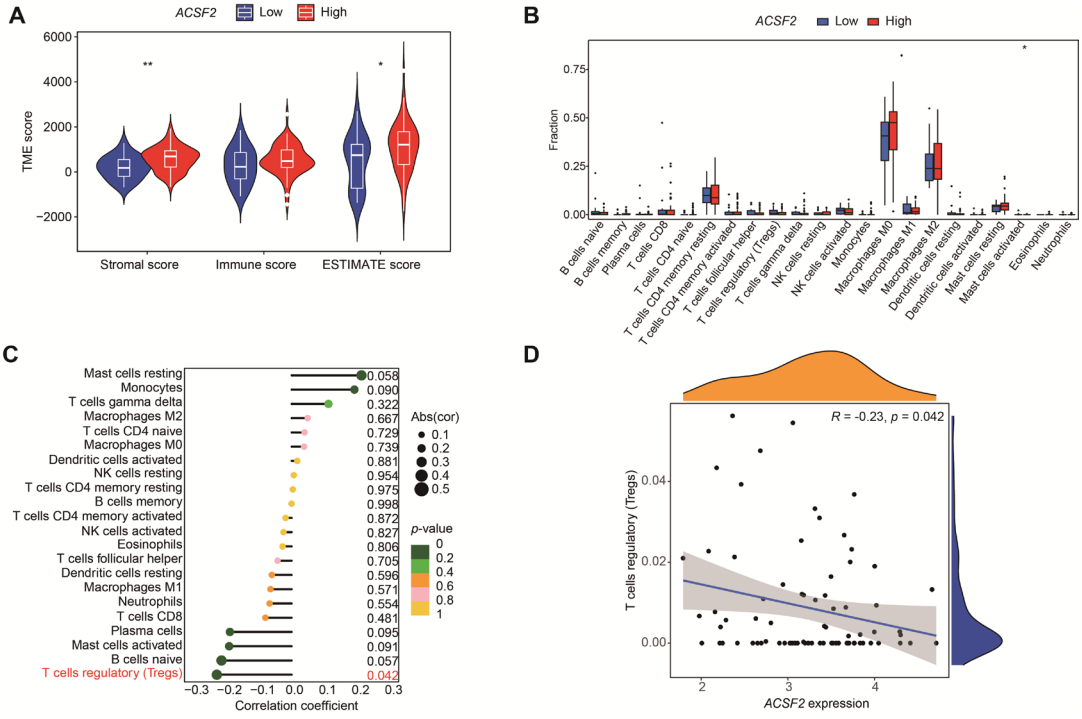


Figure 7. Associations between *ACSF2* expression and immune-related features inferred from bulk RNA-seq data. (A) Assessment of scores computationally derived from the ESTIMATE algorithm in 84 Therapeutically Applicable Research to Generate Effective Treatments–Osteosarcoma patients grouped according to the median *ACSF2* expression threshold. (B) Comparison of CIBERSORT-estimated immune-cell proportions between the two *ACSF2* expression groups. (C) Pearson-based correlation analysis assessing associations between *ACSF2* transcript abundance and the relative fractions of 22 distinct immune-cell subsets. Point position represents correlation coefficients, point magnitude reflects their absolute values, and point color encodes corresponding nominal *p*-values. (D) Correlation between *ACSF2* expression and the estimated proportion of regulatory T cells. The regression line is shown with its 95% confidence interval, and marginal plots show the variable distributions.
Notes: *nominal $p < 0.05$; **nominal $p < 0.01$.

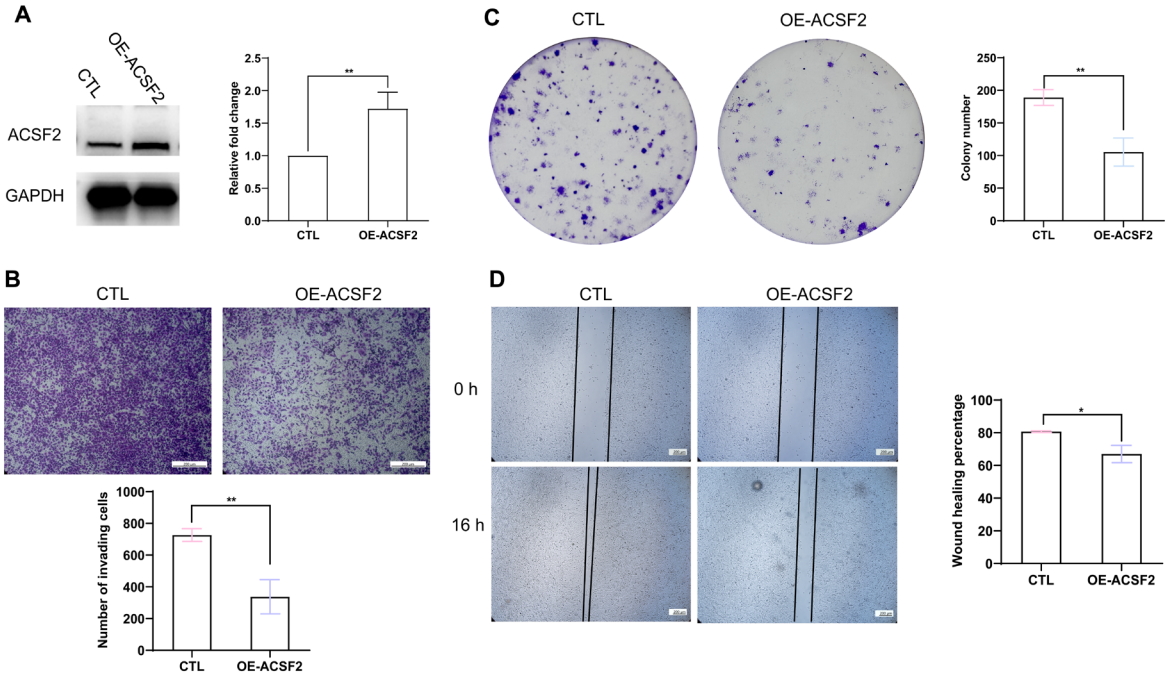


Figure 8. ACSF2 inhibits the migration, invasion, and colony formation capacities of HOS cells. (A) Immunoblotting was used to confirm the overexpression of ACSF2 in HOS cells transfected with an ACSF2 overexpression plasmid or an empty vector control. (B) Cells were seeded onto Matrigel-coated Transwell inserts and incubated for 36 h. Crystal violet staining was used to visualize cells that reached the lower surface of the membrane. Representative images, along with quantitative statistics for invaded cell counts, are shown in the left and right panels, respectively. Scale bar: 200 μm; magnification: 100×. (C) We conducted colony formation assays to compare proliferative capacity and colony-forming phenotypes of ACSF2-overexpressing HOS cells relative to control cells. Representative colony pictures and quantitative analysis of colony numbers are shown. (D) A scratch wound-healing test was applied to examine cell migration potential. Following transfection, uniform scratches were generated on confluent cell monolayers with a sterile 100 μL pipette tip. Black lines indicate the scratch edges. Scale bar: 200 μm; magnification: 40×. Representative imaging data and matching statistical analyses are provided. Notes: $^{*}p < 0.05$; $^{**}p < 0.01$; all results are reported as mean ± standard deviation.
Abbreviations: ACSF2: Acyl-CoA synthetase family member 2; CTL: Control; OE: Overexpression.

4. Discussion

As the predominant primary malignant tumor of bone, osteosarcoma possesses a high tendency for metastasis, which markedly worsens patient clinical prognosis. Fatty acid metabolism sustains cellular energy metabolism and actively modulates tumor cell proliferation and malignant progression,[10] rendering FAMRGs promising prognostic candidates for tumor research. In the present study, we integrated multi-cohort transcriptomic profiles and clinical data to screen prognosis-related FAMRGs and systematically characterize the clinical significance and biological implications of ACSF2 in osteosarcoma.

Among the 15 consistently dysregulated FAMRGs, both *ACSF2* and *PPT1* exhibited potential prognostic value in preliminary analyses. *PPT1* encodes a lysosomal depalmitoylating enzyme closely implicated in autophagy and tumor progression.[18-20] Although *PPT1* was screened as a candidate prognostic gene via LASSO regression and correlated with increased mortality risk in univariable Cox analysis, its prognostic significance failed to sustain after adjusting for sex, age, diagnostic metastatic status, and definitive surgery. Accordingly, *PPT1* was considered a preliminary candidate and excluded from subsequent prognostic modeling and experimental validation, while downstream analyses focused specifically on *ACSF2*.

Acyl-CoA synthetase family member 2 functions as a key acyl-CoA synthetase that initiates fatty acid metabolism by catalyzing thioester bond formation between fatty acids and coenzyme A. Previous studies have primarily linked ACSF2 to ferroptosis modulation and mitochondrial homeostasis in multiple non-tumor diseases, including renal ischemia–reperfusion injury, ulcerative colitis, and osteoarthritis.[21-23] However, the tumor-related roles of ACSF2 remain poorly defined and context-dependent across different malignancies. Aberrant upregulation of *ACSF2* has been reported in ovarian cancer,[24] whereas decreased *ACSF2* expression is correlated with pulmonary metastasis in differentiated

thyroid carcinoma.[25] In our study, *ACSF2* was significantly downregulated in osteosarcoma tissues relative to non-tumor controls, and patients with low *ACSF2* expression exhibited inferior OS and EFS in the TARGET-OS cohort. In this cohort, the association between *ACSF2* expression and metastasis at diagnosis was not statistically significant. Incomplete follow-up data prevented a separate analysis of its association with later metastatic relapse.

The GSEA results revealed that *ACSF2* expression was closely correlated with fatty acid metabolism and mitochondrial energy metabolic pathways. Nevertheless, these pathway-level associations are statistically exploratory and do not confirm direct regulatory effects of *ACSF2*. Drug sensitivity prediction demonstrated that elevated *ACSF2* expression was associated with lower predicted response scores for Uprosertib and MN-64, indicating enhanced drug sensitivity. This finding is consistent with the favorable survival outcomes observed in the *ACSF2*-high subgroup, although such correlations may reflect shared transcriptional or metabolic landscapes rather than direct causal effects. Uprosertib acts as a pan-AKT inhibitor, while MN-64 exerts anti-tumor activity by blocking tankyrase-mediated wingless-related integration site signaling.[26,27] Notably, neither compound represents a standard first-line therapeutic for osteosarcoma, and all drug-response results were computationally predicted via OncoPredict; therefore, their clinical translational value requires rigorous experimental verification.

Although immunotherapeutic strategies have been increasingly investigated for osteosarcoma treatment,[28-30] reliable biomarkers for precise patient stratification and immunotherapy response prediction remain lacking.[31-33] Deconvolution of bulk RNA-seq data showed a negative correlation between *ACSF2* expression and the estimated regulatory T-cell fraction. *ACSF2* expression was also associated with *CCL21*, *TNFSF4*, *ENTPD1*, and *CCR10* expression. These results preliminarily suggest a potential link between ACSF2 and tumor immune microenvironment remodeling, yet they cannot confirm direct modulation of immune infiltration or immunotherapeutic efficacy. Given that bulk transcriptomic data integrate mixed signals from tumor cells, stromal components, and bone tissue, precise tissue-level and cell-level validation is essential to clarify *ACSF2*-mediated immune regulation.[34,35]

The current study has several inherent limitations. First, due to the lack of matched normal bone or osteoblast samples in the TARGET-OS database, GTEx skeletal muscle tissues were adopted as non-tumor references, consistent with previously reported osteosarcoma transcriptomic studies.[14-17] Despite this widely accepted strategy, skeletal muscle is not a lineage-matched control, and inter-dataset and inter-tissue heterogeneity may introduce potential bias. To minimize such confounding effects, we performed independent differential expression analyses in the TARGET-OS/GTEx and GSE16088 cohorts and retained only FAMRGs with consistent dysregulation patterns across the two datasets. Second, survival analysis was restricted to 84 TARGET-OS patients with 29 recorded death events. Critical clinical information, including tumor size, histological subtype, surgical margin status, chemotherapy response, and detailed treatment regimens, was incomplete or unavailable, limiting comprehensive multivariate adjustment. Although bootstrap internal validation confirmed favorable model stability, the limited sample size and event number may lead to potential overfitting risk.[36] In addition, the optimal gene expression cut-offs were determined and validated within a single cohort, which may overestimate survival stratification efficacy; thus, these cut-off values cannot be regarded as clinically validated thresholds.[37] Third, EFS was defined based on the first-event information provided by the TARGET database. Detailed data regarding relapse sites and relapse types were unavailable, prohibiting independent analysis of late metastatic relapse events.

Furthermore, all pathway enrichment, immune infiltration, and drug response analyses should be interpreted with caution. GSEA provides macroscopic pathway correlations rather than direct causal evidence. Similarly, ESTIMATE and CIBERSORT algorithms computationally infer stromal and immune cell proportions from bulk transcriptomic data, instead of conducting direct experimental quantification, and these estimations are susceptible to the complex cellular composition of osteosarcoma tissues.[38,39] Notably, Benjamini–Hochberg multiple testing correction was only applied to GSEA, whereas differential expression screening, GO/KEGG enrichment, drug sensitivity analysis, and immune correlation analyses were based on nominal *p*-values, which may contain false-positive results.[40] In addition, direct functional assays verifying fatty acid oxidation, mitochondrial function, ferroptosis activity, immune modulation, and drug response were lacking in the present study. Therefore, the biological functions and translational implications of *ACSF2* require further validation via in-depth functional experiments and patient-derived preclinical models.[41,42]

5. Conclusion

In summary, this study identified 15 consistently dysregulated FAMRGs in osteosarcoma. Within the TARGET-OS cohort, reduced *ACSF2* expression was significantly correlated with unfavorable OS and EFS, supporting *ACSF2* as a promising prognostic biomarker

for osteosarcoma. No significant association was detected between *ACSF2* expression and initial diagnostic metastasis, and late metastatic progression was not analyzed independently. Transcriptome-based bioinformatic analyses further revealed potential correlations of *ACSF2* with metabolic reprogramming, tumor immune microenvironment characteristics, and predicted drug sensitivity. All computational findings in this study are hypothesis-generating and cannot confirm *ACSF2* as a clinically validated therapeutic target. Further rigorous functional experiments and clinical cohort validation are warranted to elucidate the biological mechanisms and translational value of *ACSF2* in osteosarcoma.

Acknowledgments

The authors thank the contributors and maintainers of the TARGET, GTEx, GEO, and UCSC Xena databases for making the data used in this study publicly available.

Funding

This study was supported by grants from the National Natural Science Foundation of China (81703557), A Project Funded by the Priority Academic Program Development of Jiangsu Higher Education Institutions (PAPD), and the College Student Innovation and Entrepreneurship Project.

Conflict of interest

The authors declare that they have no competing interests.

Author contributions

Conceptualization: Xiao Shi, Xinxin Si, and Hao Gu
Data curation: Hao Gu, Changsheng Zhang
Formal analysis: Hao Gu, Changsheng Zhang
Investigation: Yu Li, Chuanzhi Zhang
Writing–original draft: Xiao Shi
Writing–review & editing: Xiao Shi, Xinxin Si

Ethics approval and consent to participate

This study analyzed publicly available, de-identified transcriptomic and clinical data of osteosarcoma patients from the TARGET-OS repository. All data were accessed in accordance with the repository's data use agreements. No new human participants were recruited, and no identifiable private information was collected. Therefore, additional institutional ethical approval and informed consent were not required for this secondary analysis.

Consent for publication

Not applicable.

Availability of data

The datasets analyzed in this study are publicly available. TARGET-OS and GTEx data were obtained through the UCSC Xena platform, and the GSE16088 dataset was obtained from the Gene Expression Omnibus database.

AI tools statement

Artificial intelligence-assisted language polishing was utilized to improve the readability and linguistic quality of this manuscript. All study design, data analysis, result interpretation, and scientific conclusion formulation were performed exclusively by the authors. The authors supervised the whole writing process and are fully responsible for all contents of this manuscript.

References

1. Isakoff MS, Bielack SS, Meltzer P, Gorlick R. Osteosarcoma: current treatment and a collaborative pathway to success. *J Clin Oncol*. 2015;33(27):3029-3035.

   doi: 10.1200/JCO.2014.59.4895

2. Meltzer PS, Helman LJ. New horizons in the treatment of osteosarcoma. *N Engl J Med*. 2021;385(22):2066-2076.

   doi: 10.1056/NEJMra2103423

3. Sheng G, Gao Y, Yang Y, Wu H. Osteosarcoma and metastasis. *Front Oncol*. 2021;11:780264.

   doi: 10.3389/fonc.2021.780264

4. Belayneh R, Fourman MS, Bhogal S, Weiss KR. Update on osteosarcoma. *Curr Oncol Rep*. 2021;23(6):71.

   doi: 10.1007/s11912-021-01053-7

5. Panez-Toro I, Muñoz-García J, Vargas-Franco JW, *et al*. Advances in osteosarcoma. *Curr Osteoporos Rep*. 2023;21(4):330-343.

   doi: 10.1007/s11914-023-00803-9

6. Hattinger CM, Patrizio MP, Fantoni L, Casotti C, Riganti C, Serra M. Drug resistance in osteosarcoma: emerging biomarkers, therapeutic targets and treatment strategies. *Cancers (Basel)*. 2021;13(12):2878.

   doi: 10.3390/cancers13122878

7. Hanahan D, Weinberg RA. Hallmarks of cancer: the next generation. *Cell*. 2011;144(5):646-674.

   doi: 10.1016/j.cell.2011.02.013

8. Jin HR, Wang J, Wang ZJ, *et al*. Lipid metabolic reprogramming in tumor microenvironment: from mechanisms to therapeutics. *J Hematol Oncol*. 2023;16(1):103.

   doi: 10.1186/s13045-023-01498-2

9. Dai CL, Qiu ZY, Wang AQ, Yan S, Zhang LJ, Luan X. Targeting cholesterol metabolism: a promising therapy strategy for cancer. *Acta Pharmacol Sin*. 2025;46(8):2093-2104.

doi: 10.1038/s41401-025-01531-9

10. Currie E, Schulze A, Zechner R, Walther TC, Farese RV Jr. Cellular fatty acid metabolism and cancer. *Cell Metab*. 2013;18(2):153-161.

doi: 10.1016/j.cmet.2013.05.017

11. Shi Y, Yue X, Luo Q. Metabolic reprogramming in osteosarcoma. *Pediatr Discov*. 2023;1(2):e18.

doi: 10.1002/pdi3.18

12. Wu Q, Chen H, Li J. Metabolic reprogramming-related drug resistance in osteosarcoma: from molecular mechanisms to therapeutic translation. *Front Mol Biosci*. 2026;13:1928880.

doi: 10.3389/fmolb.2026.1928880

13. Qian H, Lei T, Hu Y, Lei P. Expression of lipid-metabolism genes is correlated with immune microenvironment and predicts prognosis in osteosarcoma. *Front Cell Dev Biol*. 2021;9:673827.

doi: 10.3389/fcell.2021.673827

14. Zhang Y, He R, Lei X, *et al*. A novel pyroptosis-related signature for predicting prognosis and indicating immune microenvironment features in osteosarcoma. *Front Genet*. 2021;12:780780.

doi: 10.3389/fgene.2021.780780

15. Liu S, Wu B, Li X, Zhao L, Wu W, Ai S. Construction and validation of a potent epigenetic modification-related prognostic signature for osteosarcoma patients. *J Oncol*. 2021;2021(1):2719172.

doi: 10.1155/2021/2719172

16. Gul Mohammad A, Li D, He R, *et al*. Integrated analyses of an RNA-binding protein-based signature related to tumor immune microenvironment and candidate drugs in osteosarcoma. *Am J Transl Res*. 2022;14(4):2501-2526.

17. Han J, Hu Y, Ding S, Liu S, Wang H. The analysis of the pyroptosis-related genes and hub gene TP63 ceRNA axis in osteosarcoma. *Front Immunol*. 2022;13:974916.

doi: 10.3389/fimmu.2022.974916

18. Henderson MX, Wirak GS, Zhang YQ, *et al*. Neuronal ceroid lipofuscinosis with DNAJC5/CSPα mutation has PPT1 pathology and exhibit aberrant protein palmitoylation. *Acta Neuropathol*. 2016;131(4):621-637.

doi: 10.1007/s00401-015-1512-2

19. Xu J, Su Z, Cheng X, *et al*. High PPT1 expression predicts poor clinical outcome and PPT1 inhibitor DC661 enhances sorafenib sensitivity in hepatocellular carcinoma. *Cancer Cell Int*. 2022;22(1):115.

doi: 10.1186/s12935-022-02508-y

20. Brun S, Bestion E, Raymond E, *et al*. GNS561, a clinical-stage PPT1 inhibitor, is efficient against hepatocellular carcinoma via modulation of lysosomal functions. *Autophagy*. 2022;18(3):678-694.

doi: 10.1080/15548627.2021.1988357

21. Shi H, Qi H, Xie D, *et al*. Inhibition of ACSF2 protects against renal ischemia/reperfusion injury via mediating mitophagy in proximal tubular cells. *Free Radic Biol Med*. 2023;198:68-82.

doi: 10.1016/j.freeradbiomed.2023.02.003

22. Luo L, Zhang S, Guo N, Li H, He S. ACSF2-mediated ferroptosis is involved in ulcerative colitis. *Life Sci*. 2023;313:121272.

doi: 10.1016/j.lfs.2022.121272

23. Zhang Y, Qiao Z, He M, Xia J. OGT promotes the ferroptosis of chondrocytes in osteoarthritis development via O-GlcNAcylation modification of ACSF2. *Immunol Res*. 2025;73(1):7.

doi: 10.1007/s12026-024-09567-5

24. Wang H, Cheng Q, Chang K, Bao L, Yi X. Integrated analysis of ferroptosis-related biomarker signatures to improve the diagnosis and prognosis prediction of ovarian cancer. *Front Cell Dev Biol*. 2022;9:807862.

doi: 10.3389/fcell.2021.807862

25. Peng X, Zhao H, Ye L, *et al*. Biomarker identification and risk prediction model development for differentiated thyroid carcinoma lung metastasis based on primary lesion proteomics. *Clin Cancer Res*. 2024;30(14):3059-3072.

doi: 10.1158/1078-0432.CCR-23-3806

26. Dumble M, Crouthamel MC, Zhang SY, *et al*. Discovery of novel AKT inhibitors with enhanced anti-tumor effects in combination with the MEK inhibitor. *PLoS One*. 2014;9(6):e100880.

doi: 10.1371/journal.pone.0100880

27. Narwal M, Koivunen J, Haikarainen T, *et al*. Discovery of tankyrase inhibiting flavones with increased potency and isoenzyme selectivity. *J Med Chem*. 2013;56(20):7880-7889.

doi: 10.1021/jm401463y

28. Chen C, Xie L, Ren T, Huang Y, Xu J, Guo W. Immunotherapy for osteosarcoma: fundamental mechanism, rationale, and recent breakthroughs. *Cancer Lett*. 2021;500:1-10.

doi: 10.1016/j.canlet.2020.12.024

29. Park JA, Cheung NV. Promise and challenges of T cell immunotherapy for osteosarcoma. *Int J Mol Sci*. 2023;24(15):12520.

doi: 10.3390/ijms241512520

30. Zhu J, Fan J, Xia Y, *et al*. Potential targets and applications

of nanodrug targeting myeloid cells in osteosarcoma for the enhancement of immunotherapy. *Front Pharmacol*. 2023;14:1271321.

doi: 10.3389/fphar.2023.1271321

31. Wu CC, Beird HC, Livingston JA, *et al*. Immuno-genomic landscape of osteosarcoma. *Nat Commun*. 2020;11(1):1008.

doi: 10.1038/s41467-020-14646-w

32. Tawbi HA, Burgess M, Bolejack V, *et al*. Pembrolizumab in advanced soft-tissue sarcoma and bone sarcoma (SARC028): a multicentre, two-cohort, single-arm, open-label, phase 2 trial. *Lancet Oncol*. 2017;18(11):1493-1501.

doi: 10.1016/S1470-2045(17)30624-1

33. Marinoff AE, Nathrath M, Shulman DS, *et al*. An international framework for clinical translation of molecular classifiers in osteosarcoma. *NPJ Precis Oncol*. 2026;10(1).

doi: 10.1038/s41698-026-01456-4

34. Moquin-Beaudry G, Marques Da Costa ME, Khneisser P, *et al*. Spatial transcriptomic atlas of aggressive osteosarcomas reveals shared immune landscape and targetable surface markers. *Nat Commun*. 2026;17(1).

doi: 10.1038/s41467-026-74603-x

35. Lacinski RA, Dziadowicz SA, Melemai VK, *et al*. Spatial multiplexed immunofluorescence analysis reveals coordinated cellular networks associated with overall survival in metastatic osteosarcoma. *Bone Res*. 2024;12(1):55.

doi: 10.1038/s41413-024-00359-z

36. Riley RD, Ensor J, Snell KIE, *et al*. Calculating the sample size required for developing a clinical prediction model. *BMJ*. 2020;368:m441.

doi: 10.1136/bmj.m441

37. Polley MYC, Dignam JJ. Statistical considerations in the evaluation of continuous biomarkers. *J Nucl Med*. 2021;62(5):605-611.

doi: 10.2967/jnumed.120.251520

38. Avila Cobos F, Alquicira-Hernandez J, Powell JE, Mestdagh P, De Preter K. Benchmarking of cell type deconvolution pipelines for transcriptomics data. *Nat Commun*. 2020;11(1):5650.

doi: 10.1038/s41467-020-19015-1

39. White BS, de Reyniès A, Newman AM, *et al*. Community assessment of methods to deconvolve cellular composition from bulk gene expression. *Nat Commun*. 2024;15(1):7362.

doi: 10.1038/s41467-024-50618-0

40. Rahnenführer J, De Bin R, Benner A, *et al*. Statistical analysis of high-dimensional biomedical data: a gentle introduction to analytical goals, common approaches and challenges. *BMC Med*. 2023;21(1):182.

doi: 10.1186/s12916-023-02858-y

41. Chen F, Zhang Z, Shen R, Chen M, Li G, Zhu X. Generation and characterization of patient-derived xenografts from patients with osteosarcoma. *Tissue Cell*. 2022;79:101911.

doi: 10.1016/j.tice.2022.101911

42. He A, Huang Y, Cheng W, *et al*. Organoid culture system for patient-derived lung metastatic osteosarcoma. *Med Oncol*. 2020;37(11):105.

doi: 10.1007/s12032-020-01429-y